

UC Irvine

UC Irvine Previously Published Works

Title

Novel small molecules disrupting Hec1/Nek2 interaction ablate tumor progression by triggering Nek2 degradation through a death-trap mechanism

Permalink

<https://escholarship.org/uc/item/0cj734x5>

Journal

Oncogene, 34(10)

ISSN

0950-9232

Authors

Hu, C-M
Zhu, J
Guo, XE
[et al.](#)

Publication Date

2015-03-05

DOI

10.1038/onc.2014.67

Peer reviewed



Published in final edited form as:

Oncogene. 2015 March 5; 34(10): 1220–1230. doi:10.1038/onc.2014.67.

Novel small molecules disrupting Hec1/Nek2 interaction ablate tumor progression by triggering Nek2 degradation through a death-trap mechanism

Chun-Mei Hu^{1,3}, Jiewen Zhu¹, Xuning Emily Guo¹, Wang Chen¹, Xiaolong Qiu¹, Bryan Ngo¹, Richard Chien¹, Yunyuan V. Wang¹, Connie Y. Tsai¹, Guikai Wu¹, Yoon Kim¹, Rodrigo Lopez², A. Richard Chamberlin², Eva Y.-H.P. Lee¹, and Wen-Hwa Lee^{1,3,4,*}

¹Department of Biological Chemistry, School of Medicine, University of California, Irvine. Irvine CA 92697, USA

²Department of Chemistry, University of California, Irvine. Irvine CA 92697, USA

³Genomic Research Center, Academia Sinica, Taipei, Taiwan

⁴Graduate Institute of Clinical Medical Science, China Medical University, Taichung, Taiwan

Abstract

Hec1 (Highly Expressed in Cancer 1) or Nek2 (NIMA-related kinase 2) is often overexpressed in cancers with poor prognosis. Both are critical mitotic regulators and phosphorylation of Hec1 S165 by Nek2 is required for proper chromosome segregation. Therefore, inactivation of Hec1 and Nek2 by targeting their interaction with small molecules represents an ideal strategy for tackling these types of cancers. Here, we showed that new derivatives of INH (Inhibitor for Nek2 and Hec1 binding) bind to Hec1 at amino acids 394–408 on W395, L399 and K400 residues, effectively blocking Hec1 phosphorylation on S165 by Nek2, and killing cancer cells at the nanomolar range. Mechanistically, the D-box (destruction-box) region of Nek2 specifically binds to Hec1 at amino acids 408–422, immediately adjacent to the INH binding motif. Subsequent binding of Nek2 to INH-bound Hec1 triggered proteasome-mediated Nek2 degradation, whereas the Hec1 binding defective Nek2 mutant, Nek2 R361L, resisted INH-induced Nek2 degradation. This finding unveils a novel drug-action mechanism where the binding of INHs to Hec1 forms a virtual death-trap to trigger Nek2 degradation and eventually cell death. Furthermore, analysis of the gene expression profiles of breast cancer patient samples revealed that co-elevated expressions of Hec1 and Nek2 correlated with the shortest survival. Treatment of mice with this kind of tumor with INHs significantly suppressed tumor growth without obvious toxicity. Taken together, the new INH derivatives are suitable for translation into clinical application.

*To whom correspondence and request for materials should be addressed. Wen-Hwa Lee, Department of Biological Chemistry, School of Medicine, University of California, 240 Med Sci D, Irvine, CA 92697. Phone: 949-824-4492; Fax: 949-824-9767; whlee@uci.edu.

Competing Financial Interests Statement

The authors declare no competing financial interests.

Supplementary Information

Supplementary Information, including Supplementary Materials and Methods, Supplementary Figures and Supplementary Tables, can be found with this article online.

Keywords

Hec1; Nek2; protein-protein interaction inhibitors; protein degradation; mitotic catastrophe

Introduction

Mitosis is a highly intricate process that depends on the precise coordination of microtubules, kinesins, and various kinases. Together, these molecules regulate proper spindle formation and faithful chromosome segregation in actively proliferating cells, and are often considered promising anticancer therapeutic targets¹⁻⁴. Microtubule targeting agents, like taxanes and *Vinca* alkaloids, are commonly used in wide range of cancers by inducing cell death through poisoning the spindle apparatus and inhibiting mitotic progression^{5, 6}. However, since microtubules are also a key component of neurons and rapidly cycling bone-marrow cells, these spindle poisons inevitably elicit a plethora of severe pathological side effects that include: peripheral neurotoxicity, neuropathy, and myelosuppression^{5, 7}. Therefore, there is a strong interest in developing chemical compounds that selectively inhibit mitotic kinesins (Eg5/KSP and CENP-E) or mitotic kinases (e.g., Aurora A and B) instead of microtubules. Currently, there are over forty different anti-mitotic inhibitors in various stages of preclinical and clinical trials^{4, 8-10}, which indicate that targeting mitotic apparatus is a useful strategy for treating cancer.

Hec1 was originally identified as a Rb-interacting protein¹¹, and later found to be an essential member of Ndc80 complex along with Nuf2, Spc24, and Spc25^{12, 13}. An early study using a neutralizing antibody to inactivate Hec1 indicated that Hec1 is critical for chromosome segregation¹¹. Subsequent investigations using siRNA to deplete Hec1 further supported the idea that Hec1 plays an important role in mitotic spindle checkpoint control¹⁴⁻¹⁷. Overall, Hec1 acts as a mitotic regulator to modulate several mitotic processes, including chromosome condensation, migration, and spindle assembly checkpoint (SAC) signaling^{1, 11, 14, 17, 18}.

Hec1 overexpression has been observed in a variety of human cancers and is associated with adverse clinical outcomes in primary breast cancers^{11, 19, 20}. In fact, overexpression of Hec1 in a mouse model resulted in spindle checkpoint hyperactivation and tumor formation²¹. On the other hand, depletion of Hec1 by virus-mediated RNAi effectively retarded tumor growth in mouse models^{22, 23}. Taken together, these results suggested that Hec1 is an important therapeutic target for developing novel anticancer regimen.

Since phosphorylation of Hec1 S165 by Nek2, a mitotic regulator, is critical for Hec1 function in modulating chromosome segregation^{17, 24}, the interaction between Hec1 and Nek2 during mitosis represents an ideal target for developing inhibitors that specifically disrupt this interaction. We have previously identified compounds that block the Hec1/Nek2 interaction²⁵. In this communication, we showed that the new leading compound, INH154, is highly potent in treating breast tumors with co-elevated expression of Hec1 and Nek2. We also demonstrated mechanistically, the binding of INHs to Hec1 forms a virtual death-trap to trigger Nek2 degradation and eventually cell death.

Results

Generation of new small molecules as potent Hec1 inhibitor

In previous studies we identified a small molecule, INH1, which directly binds to Hec1 and inhibits cancer growth with an IC_{50} within the 15 μ M range²⁵. To improve the drug efficacy, we first built a molecular model of Hec1 coiled-coil region by homology modeling based on the crystal structure of the coiled-coil protein Tropomyosin and then docked INH1 on this structure (Figure 1a and Supplementary Figure 1). It was noted that INH1 preferentially interacts with the first coiled-coil region of Hec1 and the thiazole moiety of INH1 showed a prominent stacking interaction with the indole moiety of Hec1 W395, which may significantly contribute to the binding with Hec1. Based on this docking model, an additional contact site consisting mainly of Hec1 residues, N396, L399, K400, and R403, was revealed (indicated by an arrow in Figure 1a). To explore the potential chemical substituents that can geometrically occupy this new site, we designed a structurally focused chemical library and prepared these compounds following a diversity-oriented synthetic scheme²⁶. Using this library, we identified INH41 as the lead compound of the second generation INH, which had IC_{50} in sub- μ M range (Table 1). Third generation of INH derivatives were generated based on INH41. Among these compounds, INH154 was the most potent inhibitor of tumor cell growth (Table 1). The IC_{50} values of INH154 in HeLa and MDA-MB-468 cancer cells were 0.20 and 0.12 μ M, respectively. In addition, both INH41 and INH154 suppressed the growth of leukemia, osteosarcoma, and glioblastoma cells, but had no significant growth inhibitory effects on non-tumorigenic fibroblast, HS27 and mammary epithelial cell, MCF10A (Figure 1b). The inactive INH22²⁵ had no growth inhibition effect on either tumor cells or normal cells (Figure 1b). Colony formation analysis further confirmed that INH41 and INH154 effectively inhibited cancer cell growth in a dose-dependent manner (Figure 1c, 1d).

INH41 and INH154 trigger mitotic catastrophe

Since inactivation of Hec1 or Nek2 was reported to trigger mitotic abnormalities, especially spindle configuration changes and chromosome misalignment^{14, 15, 17, 27-29}, we then tested whether INH41 or INH154 treatment would elicit a similar cellular phenotype. In contrast to control DMSO treatment, cells displayed increased chromosomal misalignment after 24 hrs of treatment with INH41 or INH154 (Figure 2a and 2b). Consistently, multipolar spindle configurations in the mitotic population were aggravated in a time-dependent manner after INH41 or INH154 treatment (Figure 2c and 2d). Over time, the accumulation of chromosomal and spindle abnormalities led to cell death. To determine whether mitotic abnormalities induced by INH41 or INH154 leads to apoptosis and necrosis³⁰, we performed flow cytometry with Annexin-V/Propidium Iodide (PI) staining³¹. The percentages of apoptotic and necrotic cells were higher in the INH41 or INH154-treated cells (17.4%, 9.5% and 67.6%, 14.7% respectively), compared to 1.8%, 0.4% in DMSO-treated cells and 1.9%, 1.1% in INH22-treated cells (Figure 2e). Together, these results suggested that INH41 and INH154 cause mitotic catastrophe leading to cell death.

Determining the INH-binding specificity on Hec1

To determine the region of Hec1 that mediates the binding to INH 41 and INH154, we created a series of deletion mutants in the Hec1 coiled-coil 1 region³² and performed pull-down assays using biotin-conjugated INHs (Figure 3a and 3b). As shown in Figure 3b, biotin-conjugated INH41 was able to pull down all Hec1 deletion mutants except L394-I408, suggesting that INH41 may directly bind to L394-I408 of Hec1. In contrast, biotin-conjugated negative compound, INH22, failed to pull down even WT Hec1. Furthermore, neither Nek2 nor the binding partner of Hec1, Nuf2, was pulled-down with INH41 (Figure 3b), indicating that INH preferentially bound to Hec1 instead of Nek2 or Nuf2.

Based on molecular docking, it was noted that INH41 and INH154 formed prominent contact points with Hec1 W395, L399 and K400 (Figure 3c). To validate the importance of these residues in determining INH-Hec1 interaction specificity, we conducted a biotin INH pull-down assay in cells expressing Hec1 W395A or W395A/L399A/K400A (WLK/AAA) mutants. As shown in Figure 3d, neither biotin-INH41 nor biotin-INH154 were able to bind either mutants or Nek2 (Figure 3d), indicating that Hec1 W395 is essential for interacting with INHs.

Since both mutants failed to bind INHs, one would expect that the cells expressing these mutants should acquire resistance to INH treatment. To test this possibility, we established MDA-MB-468 cells stably expressing Hec1 WT, W395A or WLK/AAA (Fig 3e) and then treated them with INHs. As shown in Figure 3f, cells expressing either Hec1 W395A or WLK/AAA showed significantly elevated IC₅₀ values for INH41 and INH154. Interestingly, expression of Hec1 triple mutant, WLK/AAA, resulted in more severe loss of growth inhibitory effect. To exclude the possibility that drug resistance was caused by inactive Hec1 functions, we measured the mitotic index in the cells overexpressing Hec1 WT, W395A, or WLK/AAA. Both Hec1 W395A and WLK/AAA had no effect on mitotic index compared to Hec1 WT, even when endogenous Hec1 was depleted. This suggests that both Hec1 mutants can maintain, at least in part, normal Hec1 function in mitosis without obvious dominant-negative effect (Supplementary Figure 2). Taken together, these findings demonstrated that INH-Hec1 binding specificity is primarily mediated by W395, and L399 and K400 also contribute to the interaction.

INHs promote Nek2 degradation and inhibit Hec1 phosphorylation on S165

To delineate the cellular consequences upon INHs treatment, we first examined Hec1 and Nek2 protein levels in INH41- or INH154- treated cells. In a time course study, Nek2 level was remarkably reduced by more than 95 % after 18 hrs of treatment with 1 μ M INH41 or INH154, while little change was observed in Hec1 expression (Figure 4a), consistent with our previous finding²⁵. Moreover, reduction of Nek2 expression was observed in two additional breast cancer cells (MDA-MB-468 and MDA-MB-231), but not non-tumorigenic mammary cell line, MCF-10A, upon INHs treatment, suggesting INHs selectively target cancer cells and not normal cells (Supplementary Figure 3 and 4). To explore the potential reasons for Nek2 expression down-regulation post-INH treatment, we performed real-time PCR analysis and observed no significant change in Nek2 mRNA level during 24 hrs of INH treatment (Supplementary Figure 5). Since Nek2 is degraded through the proteasome

pathway at prometaphase³³, we then co-treated cells with INHs and the proteasome inhibitor, MG132, and found MG132 treatment prevented the INHs-induced degradation of Nek2 (Figure 4b and c). However, INH treatment did not affect the stability of other mitotic molecules including cyclin B and two mitotic kinases, Aurora A and PLK1 (Figure 4d and Supplementary Figure 3).

Since phosphorylation of Hec1 S165 is Nek2 dependent, and has been reported to play an important role in Hec1 function^{17, 24}, it is likely that INHs treatment would also abolish Hec1 S165 phosphorylation. As predicted, the phosphorylated Hec1 levels (pS165 Hec1) were notably reduced in a time-dependent fashion upon treating cells with 1 μ M INH41 or 154 for 4 to 24 hrs (Figure 4e). In addition, immunostaining using the same phosphor-specific antibody showed a dramatic diminution in Hec1 phosphorylation signal at kinetochores after INHs treatment compared to DMSO-treated cells relative to control antibody against ACA (red) at kinetochores (Figure 4f and 4g). Collectively, these data suggested that INHs treatment inhibits Hec1 S165 phosphorylation by promoting proteasome-mediated Nek2 degradation.

Binding of INHs to Hec1 forms a virtual death-trap to trigger Hec1-bound Nek2 degradation

Next, we sought to explore how Nek2 degradation is triggered upon INHs treatment. Since both Hec1 W395A and WLK/AAA mutants exhibited resistance to INHs, it is likely that INH treatment may not induce Nek2 degradation in cells expressing these mutants. To test this possibility, we first performed a co-immunoprecipitation experiment using cells expressing Hec1 WT, W395A or WLK/AAA, and showed that both Hec1 mutants retained Nek2 interaction and Hec1 S165 phosphorylation (Figure 5a). Noticeably, upon INH treatment, cells expressing either Hec1 W395A or WLK/AAA mutant failed to induce Nek2 degradation (Figure 5b and Supplementary Figure 6). These data suggested that Nek2 degradation induced by INH is dependent on INH binding to Hec1.

Next, we employed the same Hec1 deletion mutants from Figure 2b to identify which region of Hec1 mediates the binding for Nek2. As shown in Figure 5c, the co-immunoprecipitation experiment demonstrated that region 3 (I408-L422) in Hec1 is the major interacting domain for Nek2, while region 2 (L394-I408) also contributed to the binding, albeit to a lesser extent. To examine whether Hec1-Nek2 interaction is required for INH-induced Nek2 degradation, we analyzed the change of Nek2 level after INHs treatment with depletion of endogenous Hec1 and expression of siRNA-resistant Hec1 Δ 3 mutant (I408-L422). As shown in Figure 5d, Nek2 was not susceptible to INHs-induced degradation when expressing Hec1 Δ 3 mutant, suggesting direct interaction between Hec1 and Nek2 is required for Nek2 degradation upon INH treatment.

To further verify the importance of Hec1-Nek2 interaction on INHs-induced Nek2 degradation, we needed a Nek2 mutant that failed to bind to Hec1. Hot-spot analysis of protein-protein interaction implicated that the residues within the D-box region of Nek2 may serve as a primary contact site for Hec1 binding (Supplementary Figure 7 and Supplementary Table 1). To test this possibility, we generated a D-box deletion mutant of Nek2A and performed co-immunoprecipitation experiment. As shown in Figure 5e, the Nek2A D-box deletion mutant failed to bind to Hec1, whereas Nek2A WT was able to be

co-immunoprecipitated with Hec1. To further pinpoint which residue within the Nek2A D-box region was critical for binding to Hec1, we performed Optimal Docking Area (ODA) analysis and found that Nek2A R361 appeared to be the best candidate according to the ODA value (Supplementary Table 1). We then generated a Nek2A mutant, R361L, and showed that it failed to bind to Hec1 by co-immunoprecipitation assay (Figure 5f). Consistently, similar to Hec1^{Δ3} mutant, Nek2A R361L was more resistant to INH154-induced degradation than WT Nek2A in a dose- and time-dependent manner (Figure 5g-j). These results suggested that binding of Nek2 to Hec1 is a prerequisite for INH-induced Nek2 degradation.

Based on the above data, we proposed a potential mechanism to explain this observation. As described in Figure 5k and l, first, Nek2 normally binds to Hec1 and phosphorylates Hec1 on S165 at M phase in cells (k). Second, since the binding site of INHs to Hec1 is adjacent to Nek2 binding hot-spot site, it is likely that INH-bound Hec1 alters Hec1-bound Nek2 conformation, leading to proteasome-mediated Nek2 degradation and reduction of Hec1 S165 phosphorylation (l). Although the precise conformational change of this transient state of Nek2 remains to be established, the explanation described herein represents the most logical deductions.

Co-elevated expressions of Hec1 and Nek2 are associated with the poorest survival in breast cancer patients and INHs effectively ablate this kind of tumor progression in a xenograft model

It was reported that up-regulation of Hec1 or Nek2 in breast cancer correlated with tumor initiation and progression^{20, 34–36}. To investigate whether this up-regulation is associated with patient prognosis, we analyzed the gene expression profiles of patient samples from publicly available microarray databases (Supplementary Table 2). The dataset was assembled using R/Bioconductor³⁷, containing 2851 clinically annotated samples after outlier and duplicate sample removal. Our analysis showed that the Pearson correlation coefficient between Hec1 and Nek2 expression levels is 0.67 ($p < 0.001$) among the 2851 samples, suggesting that Hec1 and Nek2 expression levels are highly associated (Figure 6a). Using a Kaplan-Meier (KM) Cox model, we analyzed the 10-year censored distant metastasis free survival (DMFS, $n=2435$) and relapse free survival (RFS, $n=1056$) probabilities of samples with Hec1 and Nek2 expression levels dichotomized at their respective median values. We found that patients with high levels of both Hec1 and Nek2 have the worst survival probability in both DMFS and RFS (Figure 6b and 6c). These results conform the concept that targeting both Hec1 and Nek2 by INH offers a useful strategy in treating human breast cancer.

To further address this possibility, we used a serial of human breast cell lines to perform Western blot analysis and INH sensitivity assay. As Shown in Supplementary Figure 8, Hec1 and Nek2 expressed higher levels in malignant breast cancer cells than in benign breast cancer MCF7 cells or non-tumorigenic mammary epithelial MCF10A cells. As expected, the cell lines with high expression levels of Hec1 and Nek2 were more sensitized to INHs treatment. Next, we used human triple negative breast cancer MDA-MB-468 cells, which expressed high levels of both Hec1 and Nek2, to test the efficacy of tumor growth in

mouse xenograft. While tumor volumes reached $\sim 100\text{mm}^3$, mice were randomly divided into 5 treatment groups and began to receive thrice-weekly intraperitoneal (i.p.) injections of vehicle control, 10 mg/kg INH41, 50 mg/kg INH41, 5 mg/kg INH154 or 20 mg/kg INH154. Treatment was continued for 6.5 weeks and the tumor sizes were measured. Tumor growth rates in mice treated with INH41 or INH154 were evidently slower than those in control animals in a dose-dependent manner (Figure 6d and 6e). Furthermore, one week after the last injections were administered, mice were sacrificed and tumors were harvested for immunohistochemistry analysis. In agreement with the tumor-growth data, the tumor proliferation index, determined by measuring BrdU staining, was clearly reduced in residual tumors treated with INH41 or INH154 in comparison with vehicle alone (Figure 6f). The expression levels of Nek2 and Hec1 S165 phosphorylation were also substantially reduced in INH41 or INH154-treated tumors than in vehicle-treated tumors (Figure 6g and 6h). Together, these results suggest that the new INH derivatives significantly suppress tumor growth in animals through the down-regulation of Nek2, and abolishment of Hec1 S165 phosphorylation. On the other hand, mice body weights were measured during the 6.5 weeks treatment period and showed little difference among treated and control groups (Supplementary Figure 9). In addition, we analyzed the toxicity of INHs by treating normal BALB/c ByJNarl mice with high dosage of INH41 (50 mg/kg) or INH154 (20 mg/kg) and showed no significant difference of body weights, blood chemistry, and complete blood count (CBC) analysis among these groups of animals (Supplementary Table 3). These data suggested that INHs treatment generates little or no toxicity.

Discussion

The mitosis-specific roles of Hec1 and Nek2, and the poor clinical association of Hec1/Nek2 overexpression with human breast cancers, make the Hec1 and Nek2 interaction an ideal target for cancer therapy. In this communication, we demonstrated that the novel INH derivatives, INH41 and INH154, which directly bind to Hec1, trigger degradation of Hec1-bound Nek2 at mitosis, impair Hec1 S165 phosphorylation, and induce mitotic catastrophe and eventual cell death. Furthermore, we found that co-elevated expression of both Hec1 and Nek2 correlated with the shortest survival in breast cancer patients and treatment with INHs effectively ablates this kind of tumor growth in a xenograft model with little or no toxicity. Thus, these compounds are suitable for translation into clinical application.

Compared to the first generation compound, INH1, our new lead compounds, INH41 and INH154, are about 20-fold or 100-fold more potent, respectively. We have previously demonstrated that the isonicotinoyl and the thiazole moieties are both essential for INH activity²⁶. The isonicotinoyl moiety is apparently involved in weak to moderate hydrogen bonds with E388 and Q392 (the distance between the pyridine nitrogen and E388 carboxyl oxygens is 4.0–4.3 Å; while the distance between the isonicotinoyl oxygen and Q392 nitrogen/oxygen atom is 3.2–4.6 Å. In addition to its hydrophobic nature, the indole side chain of W395 serves as a versatile π -donor³⁸ to electronically interact with the thiazole ring of INHs (the distance between the indole and thiazole rings in the INH154-Hec1 docking models is 3.0–3.7 Å. Guided by the docking model, more interaction points were secured to successfully increase the potency of this series of INH compounds. Particularly in INH154, the extended piperidine side chain apparently provides additional hydrophobic interactions

with the side chains of residues L399 and K400. The distances between piperidine nitrogen of INH154 and the polar atoms of N396/K400/R403 side chains are in the range of 5-7 Å in a rigid model. Considering possible side chain flexibility, the lone electron pair on this nitrogen of INH154 may serve as a hydrogen bond acceptor for donors from either one of the three Hec1 side chains. This is partly supported by the fact that amide analogues (INH146 and INH160) are generally less potent than amino/ether analogues (INH57, INH79, INH81, INH130, INH154, INH158, INH212). Further optimization based on the structure-activity relationship is certainly warranted.

Difficulties in defining clear cut protein-protein interacting interface is one of the major challenges for drug design of this kind³⁹. A successful example is probably p53/MDM2 disruptors, such as nutlins and RITA, following the unveiling of the p53-MDM2 crystal structures⁴⁰⁻⁴². These compounds structurally mimic protein interfaces to disrupt MDM2/p53 interaction, which in turn induce accumulation and reactivation of p53 in both cancer and normal cells. However, since all these compounds act through inhibiting MDM2 to restore p53 functions, they have limitation on cells with mutated or deleted p53. In the endeavor of seeking specific protein-protein interaction disruptors, we have taken a forward chemical genetics approaches and identified RAD51 inactivator⁴³ and Hec1/Nek2 disruptors²⁵. Interestingly, disruption of RAD51-BRC interaction and RAD51 multimerization by IBR2 triggers RAD51 degradation in cancer cells through proteasome pathway.

Intriguingly, INHs act through a completely different mechanism compared to either MDM2/p53 disruptors or IBR2. INHs directly bind Hec1 but induce degradation of Nek2. It is clear that this degradation is specific to Nek2, as neither Aurora A nor Plk1 was affected (Figure 4d and Supplementary Figure 3). We have shown previously that depletion of Hec1 by siRNA without drug treatment is not sufficient for Nek2 degradation²⁵, and expressing INH-binding deficient Hec1 mutant in cells retarded INH-induced Nek2 degradation (Figure 5b and Supplementary Figure 6), suggesting that Nek2 degradation is specific for INHs treatment. Importantly, the INH-induced Nek2 degradation requires direct interaction between Hec1 and Nek2. Expressing either Nek2-binding deficient Hec1 mutants or Hec1-binding deficient Nek2 mutants renders resistance to Nek2 degradation in cancer cells upon INHs treatment (Figure 5c-j). The interaction between Hec1 and Nek2 occurs specifically at G2-M phase²⁴ and INH treatment retarded G2/M progression, induced Nek2 degradation and activated apoptosis signal in cancer cells (Supplementary Figure 10). However, INH treatment did not induce Nek2 degradation at G1/S phase (Supplementary Figure 11). These findings indicate that targeting Hec1/Nek2 interaction by INHs triggered Nek2 degradation through specific temporal and spatial interaction between Hec1 and Nek2 at M phase.

How INHs-Hec1 binding triggers Nek2 degradation is of interest. Since the binding site of INHs to Hec1 is adjacent to Nek2 binding hot-spot site, it is likely that a distinct conformational change of Nek2 may take place when it binds to INHs-bound Hec1, and signal for Nek2 degradation. Thus, INH-bound Hec1 interface may cooperatively serve as a “death-trap” to entice Nek2 for degradation. Consistent to this notion, Nek2A D-box R361L mutant failed to bind Hec1 and appeared to be resistant to INHs-induced degradation. The

death-trap created by the interface of INH-bound Hec1 may provide a unique mechanism rendering the targeted protein for proteasome degradation.

Elevated Hec1 or Nek2 levels have been detected in many types of aggressive tumors^{34, 44–46} and correlated with poor prognosis as well as resistance to chemotherapy⁴⁷. Consistently, we found that the high expression levels of both Hec1 and Nek2 strongly correlated with the shortest survivals based on the analysis of clinical breast cancer patient data (Figure 6a, b and c). Our innovative INH41 and INH154 not only inactivate Hec1, but also induce degradation of mitotic kinase Nek2, may emerge as powerful cancer therapeutic for Nek2 and Hec1 overexpressing cancers.

Materials and methods

Chemistry

INHs and biotin-conjugated INHs were synthesized at the Synthesis Facility, University of California at Irvine. See Supplementary Methods for synthetic schemes and procedures.

Cell lines and establishment of stable cell lines

Human breast cancer cell lines (MDA-MB-231 and MDA-MB-468), osteosarcoma line (U2OS), cervical adenocarcinoma line (HeLa) and normal skin fibroblast (Hs27) were maintained in DMEM medium (Invitrogen, Grand Island, NY) supplemented with 10% fetal bovine serum (FBS) and 1% penicillin-streptomycin. The leukemia cell line (K562) and glioblastoma cell line (T98G) were grown in RPMI 1640 supplemented 10% FBS and 1% penicillin-streptomycin. Normal mammary epithelial cell line (MCF10A) was cultured in DMEM/F12 (50:50) supplemented with 5% horse serum, 0.1 µg/mL cholera toxin, µg/mL insulin, µg/mL hydrocortisone, and 20 ng/mL epidermal growth factor. To establish MDA-MB-468 cells that stably expressed each individual GFP-Hec1 constructs, cells were infected with respective retrovirus, and were selected with µg/mL puromycin.

Molecular Docking

Receptor structure of Hec1 coiled-coil region was obtained by homology modeling using ICM Pro (Molsoft L.L.C, San Diego, CA), based on the crystal structure of the coiled-coil protein Tropomyosin (PDB Accession No: 1C1G, see Supplementary Methods and Supplementary Figure 1). Receptor pocket was identified using the automatic pocket finder of ICM Pro, and the largest pocket (Residues E375, Q378 - L418, R420, K431, L434, I435; Volume = 2,492 Å³) was used for docking of small compounds. INHs structures were generated and optimized using the Molecular Editor in ICM Pro⁴⁸. Interactive docking was performed using ICM Pro, with the default setting (thoroughness = 1), and the docked conformations with lowest energy were chosen for further analysis.

Biotin-INHs pull-down assay

Cells expressing GFP-Hec1 were lysed and subjected for sonication in Lysis 125 buffer. Cell extract was first pre-clared with neutravidin-resin (Thermo Fisher Scientific Inc., Waltham, MA), and then incubated with the neutravidin-resin conjugated with compound-biotin for 3 hrs at 4°C. The resin was then collected, and washed with 50 resin volumes

washing buffer (Lysis 125 buffer with 0.15% trion-x-100). Finally, the proteins on resin were eluted with 2x SDS loading buffer by boiling the resin for 10 min at 95°C heat plate. The supernatants were subjected to SDS-PAGE and Western blot analysis.

Immunoprecipitation

Over 80% confluent cells in 10 cm Petri dish were lysed in 1 mL Lysis 125 buffer (50 mM Tris, pH 7.4, 125 mM NaCl, 5 mM ethylenediaminetetraacetic acid [EDTA], 5 mM EGTA, 0.1% Nonidet P-40, 50 mM NaF, 1 mM phenylmethylsulfonyl fluoride [PMSF], 500 nM Microcystin-LR, and 1x proteinase inhibitor cocktail (Roche, Indianapolis, IN)) and subjected to three liquid nitrogen freeze–thaw cycles. Lysate was pre-clarified by incubating with Protein G Sepharose (pre-blocked with 5 % BSA/PBS for 2 hrs) for 1 hr at 4°C. Clarified lysate was then removed from the beads and incubated with antibodies at 4°C for 2 hrs, followed by incubation of fresh Protein G Sepharose for 1 hr at 4°C. Immunoprecipitates were washed three times with wash buffer (50 mM Tris, pH 7.4, 125 mM NaCl, 5 mM EDTA, 5 mM EGTA, 0.1% Nonidet P-40, 50 mM NaF, and 1 mM PMSF). The lysates and immunoprecipitates were separated by SDS–PAGE, and subjected to Western blot analysis.

Xenograft mice studies

All mice experiments were performed under the guidelines of the University of California at Irvine Animal Research Committee. Athymic nude mice (nu/nu; Harlan Sprague-Dawley Inc., Indianapolis, IN) were maintained in pathogen-free conditions within the University Laboratory Animal Resources Center at the University of California Irvine according to approved institutional protocols. MDA-MB-468 breast cancer cells (2×10^6) were injected into the mammary fat pads of 6- to 8-wk-old nude mice. Once tumors reach $\sim 100\text{mm}^3$, mice were divided into 5 treatment groups (n=6 per group): vehicle control (5% DMSO, 7.5% Ethanol, 7.5% Cremophor EL, 20% PEG400, 60% saline), 10 mg/kg INH41, 50 mg/kg INH41, 5 mg/kg INH154 or 20 mg/kg INH154. Mice were treated with vehicle control or INHs thrice weekly via i.p. injection. Mice body weights and tumor sizes were measured twice weekly. Tumor volume was calculated as $(\text{length} \times \text{width}^2)/2$ (in mm), and data were presented as mean tumor volume \pm SEM.

Statistical Analyses

A two-tailed Student's t test was used to tumor growth, immunostaining analysis, immunohistochemistry for pS165 Hec1, BrdU staining and IC_{50} for INH41 or INH154 in MDA-MB-468 cells stably expressing GFP-Hec1 mutants. *, ** indicate $p < 0.05$ and $p < 0.01$, respectively.

All other experimental procedures are described in the Supplementary Material and Methods.

Supplementary Material

Refer to Web version on PubMed Central for supplementary material.

Acknowledgments

We thank the initial efforts by Guideng Li, Randy Wei and Yumay Chen on this project. This work was supported by NIH grant (CA107568) to WHL

References

1. Foley EA, Kapoor TM. Microtubule attachment and spindle assembly checkpoint signalling at the kinetochore. *Nat Rev Mol Cell Biol.* 2013; 14:25–37. [PubMed: 23258294]
2. Walczak CE, Cai S, Khodjakov A. Mechanisms of chromosome behaviour during mitosis. *Nat Rev Mol Cell Biol.* 2010; 11:91–102. [PubMed: 20068571]
3. Rath O, Kozielski F. Kinesins and cancer. *Nat Rev Cancer.* 2012; 12:527–539. [PubMed: 22825217]
4. Chan KS, Koh CG, Li HY. Mitosis-targeted anti-cancer therapies: where they stand. *Cell Death Dis.* 2012; 3:e411. [PubMed: 23076219]
5. Jordan M, Wilson L. Microtubules as a Target for Anticancer Drugs. *Nat Rev Cancer.* 2006; 4:253–265. [PubMed: 15057285]
6. Perez EA. Microtubule inhibitors: Differentiating tubulin-inhibiting agents based on mechanisms of action, clinical activity, and resistance. *Mol Cancer Ther.* 2009; 8:2086–2095. [PubMed: 19671735]
7. Rowinsky E. The Development and Clinical Utility of the Taxane Class of Antimicrotubule Chemotherapy Agents. *Annu Rev Med.* 1997; 48:353–374. [PubMed: 9046968]
8. Sakowicz R, et al. Antitumor activity of a kinesin inhibitor. *Cancer Res.* 2004; 64:3276–3280. [PubMed: 15126370]
9. Schmit TL, Ahmad N. Regulation of mitosis via mitotic kinases: new opportunities for cancer management. *Mol Cancer Ther.* 2007; 6:1920–1931. [PubMed: 17620424]
10. Jackson JR, Patrick DR, Dar MM, Huang PS. Targeted anti-mitotic therapies: can we improve on tubulin agents? *Nat Rev Cancer.* 2007; 7:107–117. [PubMed: 17251917]
11. Chen Y, Riley DJ, Chen PL, Lee WH. HEC, a novel nuclear protein rich in leucine heptad repeats specifically involved in mitosis. *Mol Cell Biol.* 1997; 17:6049–6056. [PubMed: 9315664]
12. Sundin LJ, Guimaraes GJ, Deluca JG. The NDC80 complex proteins Nuf2 and Hec1 make distinct contributions to kinetochore-microtubule attachment in mitosis. *Mol Biol Cell.* 2011; 22:759–768. [PubMed: 21270439]
13. Umbreit NT, et al. The Ndc80 kinetochore complex directly modulates microtubule dynamics. *Proc Natl Acad Sci U S A.* 2012; 109:16113–16118. [PubMed: 22908300]
14. Martin-Lluesma S, Stucke VM, Nigg EA. Role of Hec1 in spindle checkpoint signaling and kinetochore recruitment of Mad1/Mad2. *Science.* 2002; 297:2267–2270. [PubMed: 12351790]
15. Meraldi P, Draviam VM, Sorger PK. Timing and checkpoints in the regulation of mitotic progression. *Dev Cell.* 2004; 7:45–60. [PubMed: 15239953]
16. Lin YT, Chen Y, Wu G, Lee WH. Hec1 sequentially recruits Zwint-1 and ZW10 to kinetochores for faithful chromosome segregation and spindle checkpoint control. *Oncogene.* 2006; 25:6901–6914. [PubMed: 16732327]
17. Wei R, Ngo B, Wu G, Lee WH. Phosphorylation of the Ndc80 complex protein, HEC1, by Nek2 kinase modulates chromosome alignment and signaling of the spindle assembly checkpoint. *Mol Biol Cell.* 2011; 22:3584–3594. [PubMed: 21832156]
18. DeLuca JG, et al. Kinetochore microtubule dynamics and attachment stability are regulated by Hec1. *Cell.* 2006; 127:969–982. [PubMed: 17129782]
19. van 't Veer LJ, et al. Gene expression profiling predicts clinical outcome of breast cancer. *Nature.* 2002; 415:530–536. [PubMed: 11823860]
20. Glinsky GV, Berezovska O, Glinskii AB. Microarray analysis identifies a death-from-cancer signature predicting therapy failure in patients with multiple types of cancer. *J Clin Invest.* 2005; 115:1503–1521. [PubMed: 15931389]
21. Diaz-Rodriguez E, Sotillo R, Schvartzman JM, Benezra R. Hec1 overexpression hyperactivates the mitotic checkpoint and induces tumor formation in vivo. *Proc Natl Acad Sci U S A.* 2008; 105:16719–16724. [PubMed: 18940925]

22. Li L, et al. Development of recombinant adeno-associated virus vectors carrying small interfering RNA (shHec1)-mediated depletion of kinetochore Hec1 protein in tumor cells. *Gene Ther.* 2007; 14:814–827. [PubMed: 17330085]
23. Gurzov EN, Izquierdo M. RNA interference against Hec1 inhibits tumor growth in vivo. *Gene Ther.* 2006; 13:1–7. [PubMed: 16121206]
24. Chen Y, Riley DJ, Zheng L, Chen PL, Lee WH. Phosphorylation of the mitotic regulator protein Hec1 by Nek2 kinase is essential for faithful chromosome segregation. *J Biol Chem.* 2002; 277:49408–49416. [PubMed: 12386167]
25. Wu G, et al. Small molecule targeting the Hec1/Nek2 mitotic pathway suppresses tumor cell growth in culture and in animal. *Cancer Res.* 2008; 68:8393–8399. [PubMed: 18922912]
26. Qiu XL, et al. Synthesis and biological evaluation of a series of novel inhibitor of Nek2/Hec1 analogues. *J Med Chem.* 2009; 52:1757–1767. [PubMed: 19243176]
27. Fry AM, Meraldi P, Nigg EA. A centrosomal function for the human Nek2 protein kinase, a member of the NIMA family of cell cycle regulators. *EMBO J.* 1998; 17:470–481. [PubMed: 9430639]
28. Fry AM. The Nek2 protein kinase: a novel regulator of centrosome structure. *Oncogene.* 2002; 21:6184–6194. [PubMed: 12214248]
29. Hayward DG, Fry AM. Nek2 kinase in chromosome instability and cancer. *Cancer Lett.* 2006; 237:155–166. [PubMed: 16084011]
30. Vitale I, Galluzzi L, Castedo M, Kroemer G. Mitotic catastrophe: a mechanism for avoiding genomic instability. *Nature reviews Mol Cell Biol.* 2011; 12:385–392.
31. Schmid I, Uittenbogaart CH, Giorgi JV. Sensitive method for measuring apoptosis and cell surface phenotype in human thymocytes by flow cytometry. *Cytometry.* 1994; 15:12–20. [PubMed: 7512891]
32. Ngo B, et al. Complementary interhelical interactions between three buried Glu-Lys pairs within three heptad repeats are essential for Hec1-Nuf2 heterodimerization and mitotic progression. *J Biol Chem.* 2013; 288:34403–34413. [PubMed: 24129578]
33. Hames RS, Wattam SL, Yamano H, Bacchieri R, Fry AM. APC/C-mediated destruction of the centrosomal kinase Nek2A occurs in early mitosis and depends upon a cyclin A-type D-box. *EMBO J.* 2011; 20:7117–7127. [PubMed: 11742988]
34. Hayward DG, et al. The centrosomal kinase Nek2 displays elevated levels of protein expression in human breast cancer. *Cancer Res.* 2004; 64:7370–7376. [PubMed: 15492258]
35. Wang S, et al. Nek2A contributes to tumorigenic growth and possibly functions as potential therapeutic target for human breast cancer. *J Cell Biochem.* 2012; 113:1904–1914. [PubMed: 22234886]
36. Bieche I, et al. Expression analysis of mitotic spindle checkpoint genes in breast carcinoma: role of NDC80/HEC1 in early breast tumorigenicity, and a two-gene signature for aneuploidy. *Mol Cancer.* 2011; 10:23. [PubMed: 21352579]
37. Carey DMB, Bolstad B, Dettling M, Dudoit S, Ellis B, Gautier L, Ge Y, et al. Bioconductor: Open software development for computational biology and bioinformatics R. Gentleman, V. J. *Genome Biol.* 2004; 5:R80. [PubMed: 15461798]
38. Hu J, Barbour LJ, Gokel GW. The indole side chain of tryptophan as a versatile pi-donor. *J Am Chem Soc.* 2012; 124:10940–10941. [PubMed: 12224916]
39. Arkin MR, Wells JA. Small-molecule inhibitors of protein-protein interactions: progressing towards the dream. *Nat Rev Drug Discov.* 2004; 3:301–317. [PubMed: 15060526]
40. Issaeva N, et al. Small molecule RITA binds to p53, blocks p53-HDM-2 interaction and activates p53 function in tumors. *Nat Med.* 2004; 10:1321–1328. [PubMed: 15558054]
41. Shangary S, Wang S. Small-molecule inhibitors of the MDM2-p53 protein-protein interaction to reactivate p53 function: a novel approach for cancer therapy. *Annu Rev Pharmacol Toxicol.* 2009; 49:223–241. [PubMed: 18834305]
42. Vassilev LT, et al. In vivo activation of the p53 pathway by small-molecule antagonists of MDM2. *Science.* 2004; 303:844–848. [PubMed: 14704432]
43. Zhu J, et al. A novel small molecule RAD51 inactivator overcomes imatinib-resistance in chronic myeloid leukaemia. *EMBO Mol Med.* 2013; 5:353–365. [PubMed: 23341130]

44. Kokuryo T, et al. Nek2 as an effective target for inhibition of tumorigenic growth and peritoneal dissemination of cholangiocarcinoma. *Cancer Res.* 2007; 67:9637–9642. [PubMed: 17942892]
45. Barbagallo F, et al. Increased expression and nuclear localization of the centrosomal kinase Nek2 in human testicular seminomas. *J Pathol.* 2009; 217:431–441. [PubMed: 19023884]
46. Andreasson U, et al. Identification of molecular targets associated with transformed diffuse large B cell lymphoma using highly purified tumor cells. *Am J Hematol.* 2009; 84:803–808. [PubMed: 19844990]
47. Zhou W, et al. NEK2 induces drug resistance mainly through activation of efflux drug pumps and is associated with poor prognosis in myeloma and other cancers. *Cancer cell.* 2013; 23:48–62. [PubMed: 23328480]
48. Cavasotto CN, Orry AJ, Abagyan RA. Structure-based identification of binding sites, native ligands and potential inhibitors for G-protein coupled receptors. *Proteins.* 2003; 51:423–433. [PubMed: 12696053]

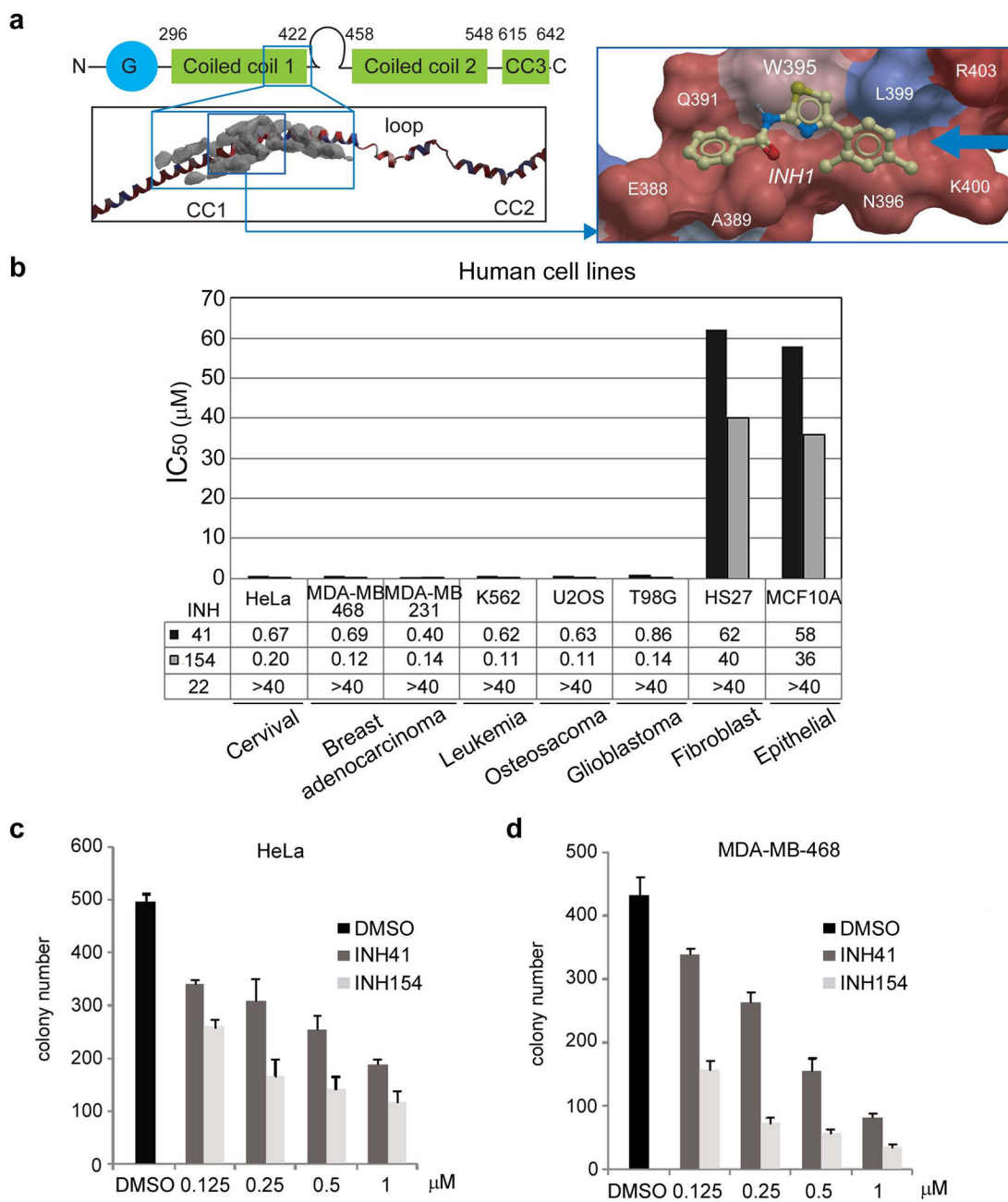


Figure 1. New potent derivatives of INH

(a) Docking model for INH1-Hec1. *Left*, computationally predicted binding site of Hec1 for INH1, indicated with grey mesh. *Right*, conformation docked with the lowest energy. INH1 was shown in ball-and-stick model and colored by element (yellow: carbon; golden: sulfur; blue: nitrogen; red: oxygen). Receptor (Hec1) surface was colored according to hydrophobicity (red to blue: increasing hydrophobicity). Residues in close proximity to INH1 were indicated in boxes. (b) IC_{50} of INH41, INH154, and INH22 on a variety of human cell lines (c-d) Colony formation assays for HeLa and MDA-MB-468 cells treated with various doses of INH41 and INH154.

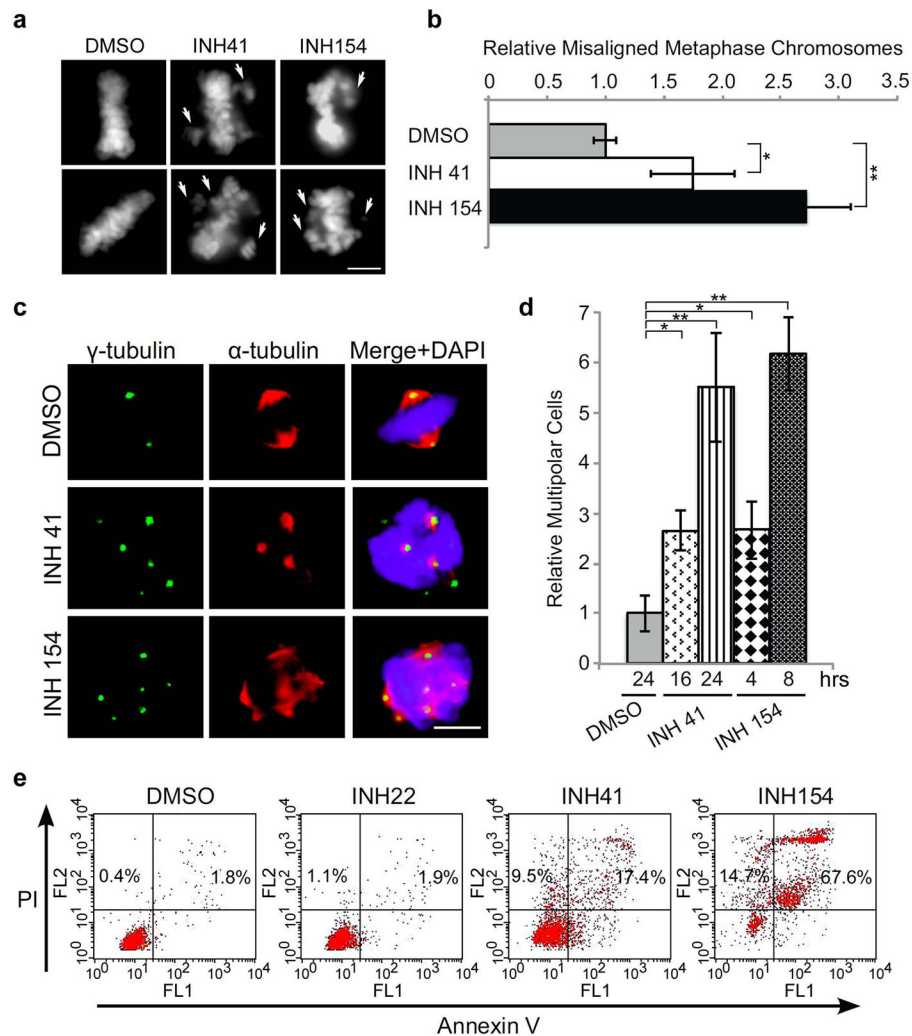


Figure 2. INHs trigger mitotic catastrophe

(a-b) Representative images and quantitation of misaligned metaphase chromosomes in HeLa cells treated with DMSO, 200 nM of INH41 or INH154 for 24 hrs. Chromosome was stained with Hoechst 33342. Data show relative fold difference in misaligned metaphase chromosomes. Error bar represent SE, $n > 200$ per sample. Scale bar, 10 μ m. Arrows indicate misaligned chromosome. (c-d) Representative images and quantitation of multipolar cells in HeLa treated with DMSO, 200 nM of INH41 or INH154. Centrosome, microtubules and chromosome were stained with anti- γ -tubulin, anti- α -tubulin and DAPI, respectively. Data show relative fold difference in multipolar cells \pm SE, $n > 200$ per sample. Scale bar, 5 μ m. (e) Apoptotic analyses of HeLa cells treated with DMSO or 1 μ M of INH22, INH41 or INH154 for 48 hrs. Percentage of apoptotic cells that were gated as PI-positive and Annexin V-positive.

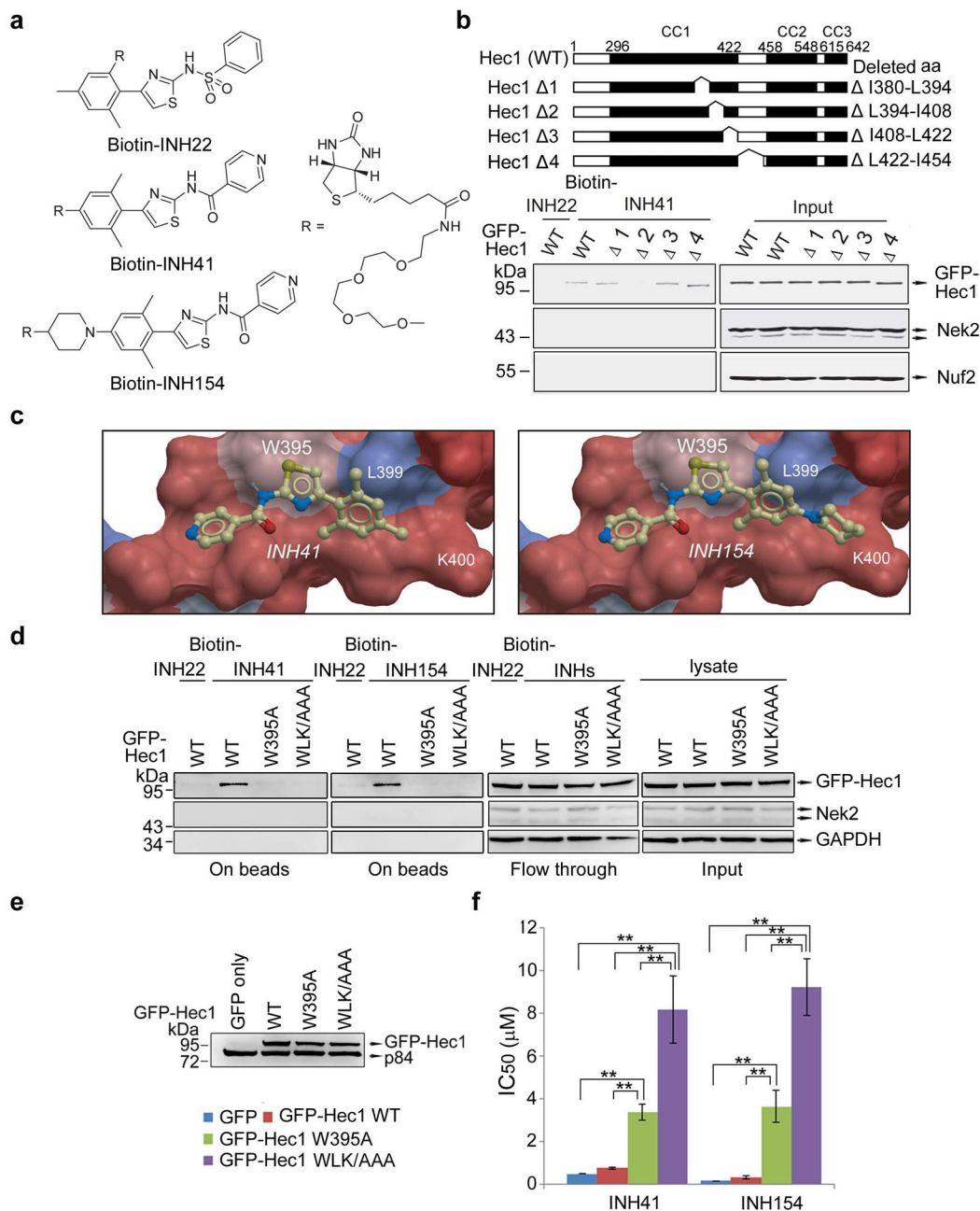


Figure 3. INHs specifically interact with Hec1 amino acids W395, L399, K400

(a) Chemical structures of biotin-conjugated INH22, INH41 and INH154. (b) *Top*, schematic diagram of GFP-Hec1 deletion mutants. *Bottom*, Affinity pull-down of Hec1 deletion mutants using biotin-INH41- or biotin-INH22-conjugated matrix from HeLa cell extract expressing respective constructs. (c) Docking models of INH41 or INH154 with Hec1. Small molecules were colored by element (yellow: carbon; golden: sulfur; blue: nitrogen; red: oxygen); receptor surfaces were colored according to hydrophobicity (red to blue: increasing hydrophobicity). Key residues in contact with the small molecules were labeled. (d) Affinity pull-down assay with biotin-INH41-, biotin-INH154 or biotin-INH22-

conjugated matrix from cells expressing GFP-Hec1 WT, W395A or WLK/AAA. INHs indicated INH41 and INH154. **(e)** Western blot analysis of GFP-Hec1 level with anti-GFP antibody in MDA-MB-468 cells stably expressing GFP, GFP-Hec1 WT, W395A, or WLK/AAA. P84 served as a loading control. **(f)** IC₅₀ of MDA-MB-468 cells stably expressing GFP, GFP-Hec1 WT, W395A, or WLK/AAA upon INH treatments. Data expressed as mean \pm SD of three independent experiments.

Author Manuscript

Author Manuscript

Author Manuscript

Author Manuscript

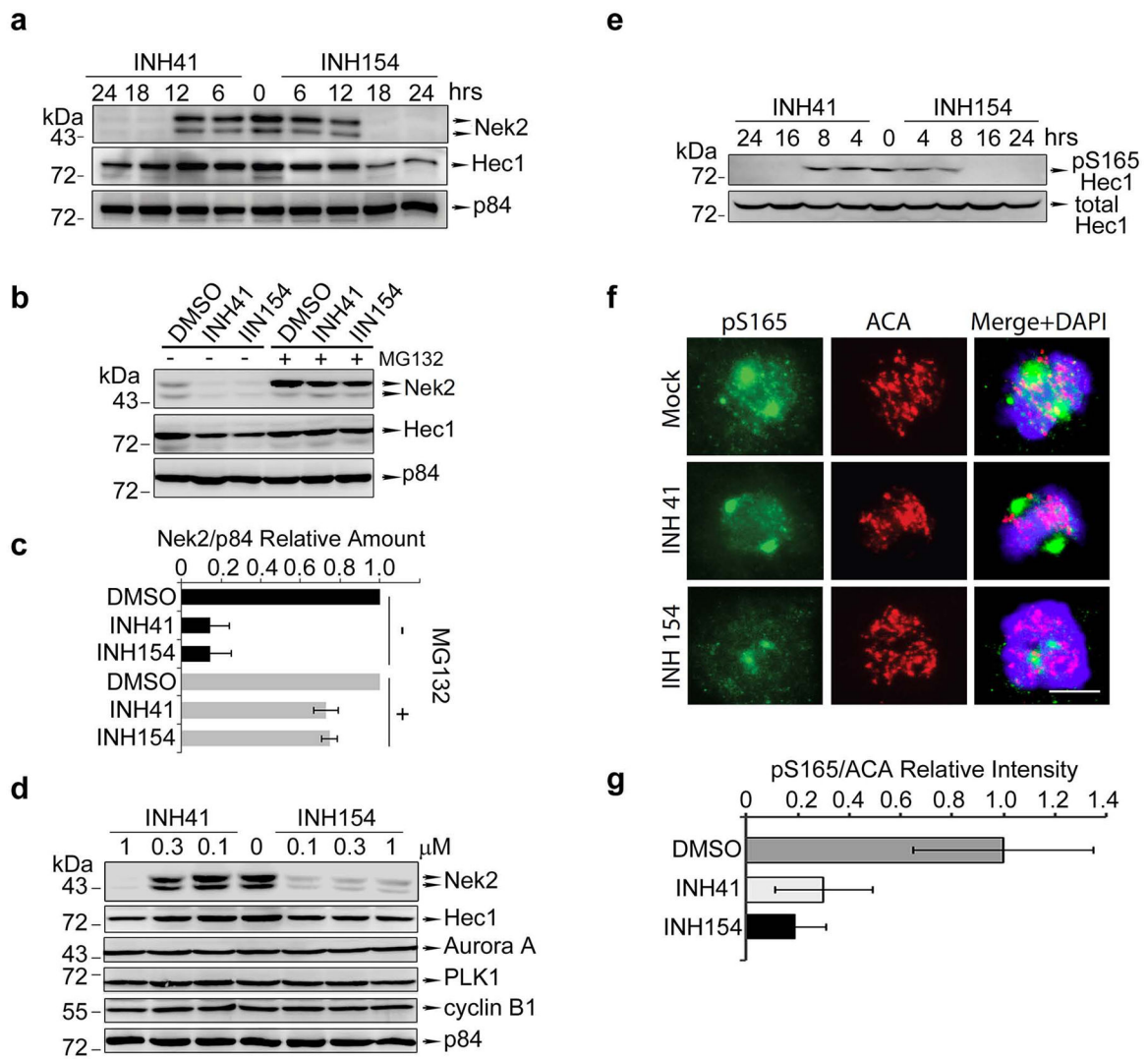


Figure 4. INH41 and INH154 treatment triggers Nek2 degradation and blocks Hec1 S165 phosphorylation

(a) Western blot analysis of Nek2 level in HeLa cells treated with 1 μ M of INH41 or INH154 for various durations as indicated. P84 served as a loading control. (b-c) Representative images of Western blot analysis and quantitation of relative Nek2 protein level in HeLa cells treated with DMSO, 1 μ M of INH41 or 1 μ M of INH154 alone or with 20 μ M of MG132 for 18 hrs. Nek2 protein level was quantitated by GEL-PRO32 software and normalized with p84. Data showed relative protein level of Nek2 \pm SD, n = 3 per sample. (d) Western blot analysis of different mitotic proteins in HeLa cells treated with various doses of INH41 or INH154 for 18 hrs. P84 served as a loading control. (e) Western blot analysis of total Hec1 and pS165 Hec1 levels in HeLa cells treated with 1 μ M of INH41 or INH154 for indicated time durations. (f-g) Representative images and quantitation of pS165/ACA intensity in HeLa cells treated with DMSO, 200 nM of INH41 or INH154 for 32 hrs. Data showed relative pS165/ACA mean intensity \pm SE. n > 20 per sample. Scale bar, 5 μ m.

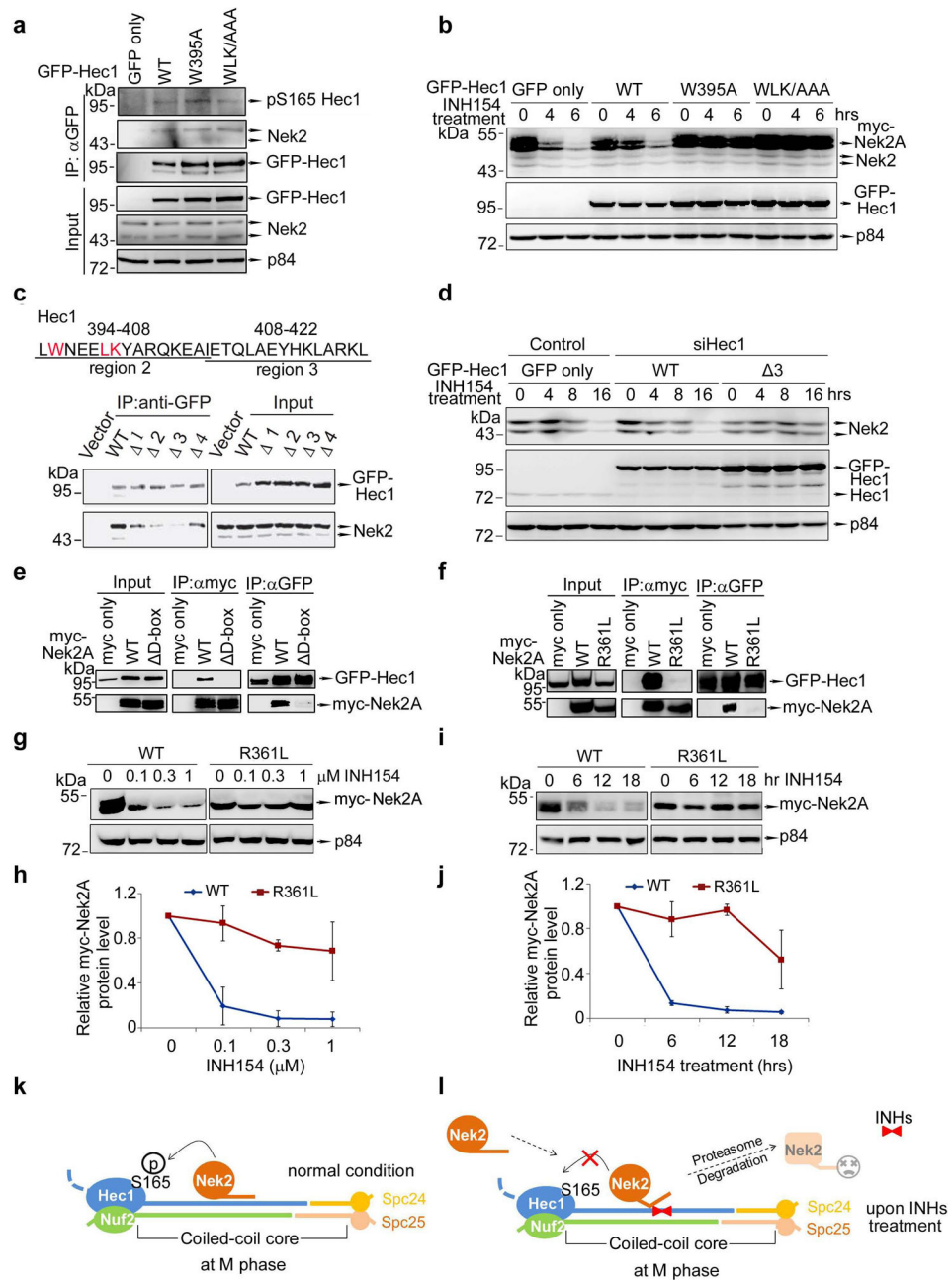


Figure 5. Mechanistic process of INH-induced Nek2 degradation

(a) Hec1 W395A and WLK/AAA retain Nek2 binding and can be phosphorylated at S165. Immunoprecipitation of GFP, GFP-Hec1 WT, W395A, and WLK/AAA using anti-GFP antibody were analyzed by Western blot with specific antibodies as indicated. (b) Hec1 W395A and WLK/AAA mutants resist INH-induced Nek2 degradation. MDA-MB-468 cells expressing GFP, GFP-Hec1 WT, W395A, or WLK/AAA, and Myc-Nek2A WT were analyzed by Western blot with anti-Nek2 and anti-GFP antibodies after treatment with 1 μ M of INH154 for the indicated time durations. (c) Deletion of Hec1 amino acids 408–422 abolishes Hec1-Nek2 interaction. Immunoprecipitation of GFP-Hec1 1, 2, or 3

expressed in HeLa cells using anti-GFP antibody. **(d)** Hec1^{Δ3} mutant resists INH-induced Nek2 degradation. Nek2, endogenous Hec1 and GFP-Hec1 protein levels in cells expressing GFP, GFP-Hec1 WT or ^{Δ3} were determined by Western blot analysis with indicated antibodies after treatment with 1 μM of INH154 at different time points. **(e-f)** Nek2 R361 is essential for Nek2-Hec1 Interaction. Myc-Nek2A WT, ^{ΔD-box}, or R361L, and GFP-Hec1 WT were co-expressed in cells for 48 hrs and co-immunoprecipitated with either anti-Myc or anti-GFP antibodies. **(g-j)**. Nek2 R361L resists INH154-induced Nek2 degradation. HeLa cells expressing Myc, Myc-Nek2A WT, or R361L were treated with 0.1-1 μM of INH154 for 18 hrs **(g-h)** or 1 μM of INH154 for indicated time points **(i-j)**. Relative protein expression level of Myc-Nek2A protein was quantitated by GEL-PRO32 software and normalized with p84. Relative protein expression level of Myc-Nek2 ± SD, n = 3 per sample. **(k-l)** Death-trap model. Under normal condition, Nek2 binds to Hec1 and phosphorylates Hec1 on S165 at M phase **(k)**. Binding of INHs to Hec1 in Hec1/Nek2 complex induces Nek2 conformational change, promotes proteasome-mediated Nek2 degradation and reduces phosphorylation of Hec1 S165 **(l)**.

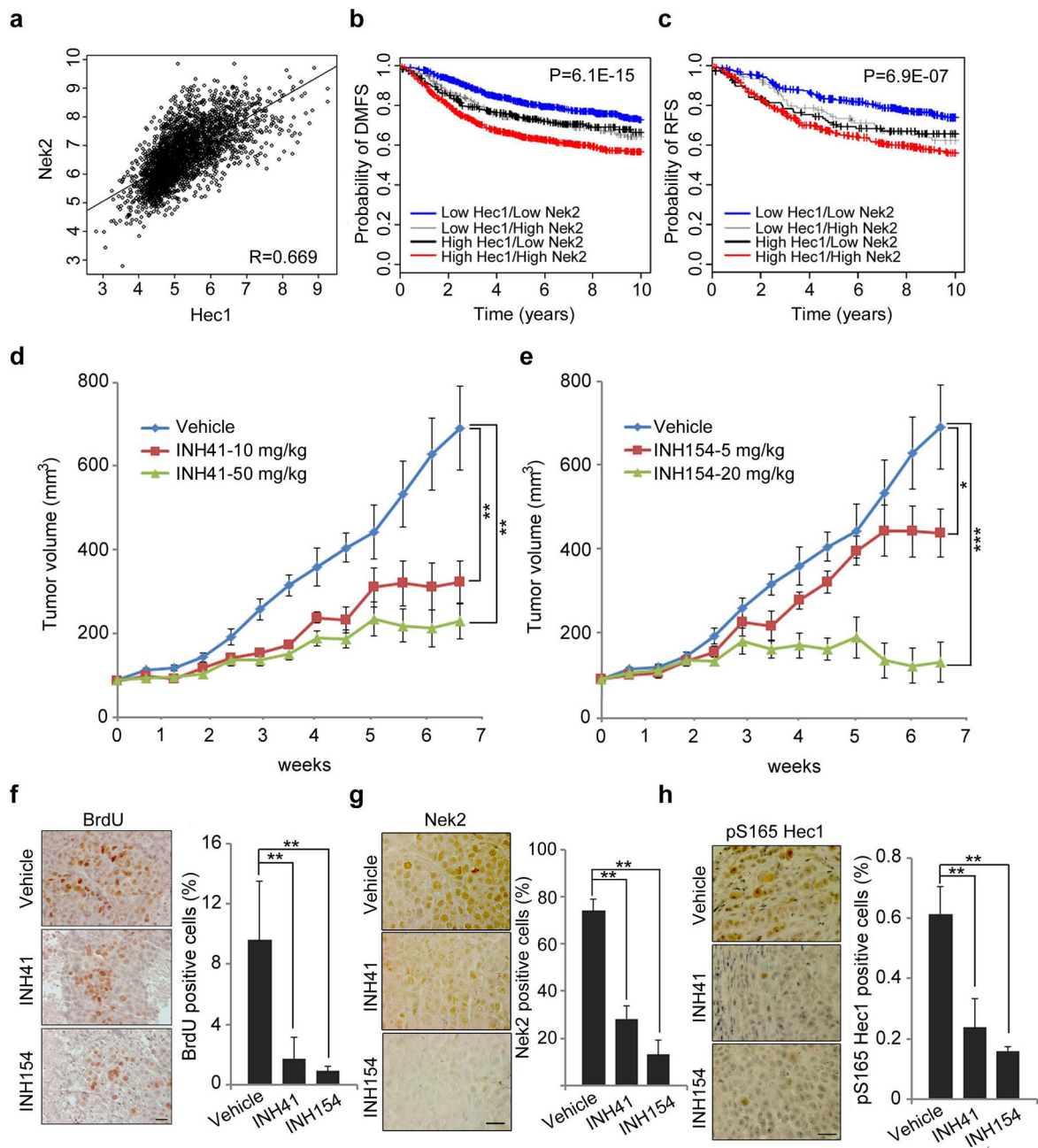


Figure 6. INH41 and INH154 effectively ablate growth of Hec1-Nek2 overexpressed breast tumors

(a) Pearson correlation of Hec1 and Nek2 expression. A total of 2849 samples were used for analysis. P value < 2.2E-16. (b) KM COX PH survival plot for distant metastasis free survival (DMFS). (c) KM COX PH survival plot ratios for relapse free survival (RFS). (d-e) Tumor sizes of athymic nude mice carrying MDA-MB-468 xenografts treated with the control vehicle or various doses of INH41 and INH154 as indicated. Error bar represent SEM (n=7). (f-h) Representative images derived from immunohistochemistry staining with

antibodies against BrdU, Nek2, and pS165 Hec1. Scale bar, 20 μ m. All error bars represent SD (n=4).

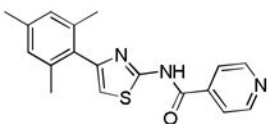
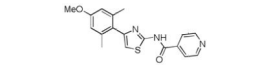
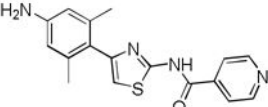
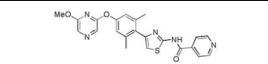
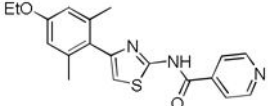
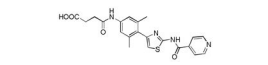
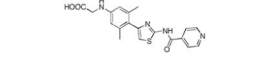
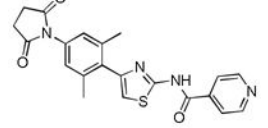
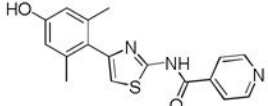
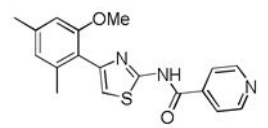
Author Manuscript

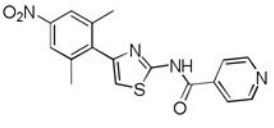
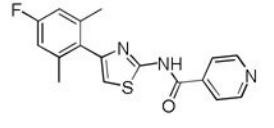
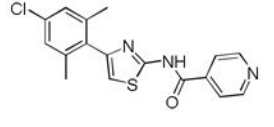
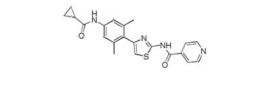
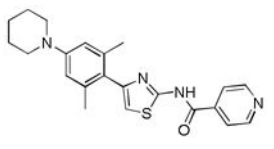
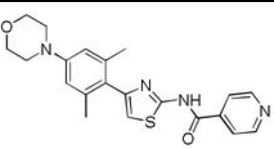
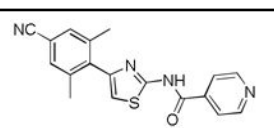
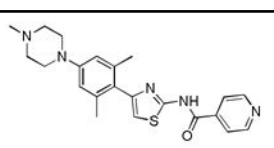
Author Manuscript

Author Manuscript

Author Manuscript

Table 1
Structures and the inhibitory activities, IC₅₀, of novel INH derivatives in HeLa and MDA-MB-468 cell lines

ID	Structure	IC ₅₀ (μM)	
		HeLa	MB468
INH41		0.67	0.69
INH57		0.39	0.25
INH79		2.3	3.2
INH81		1.4	0.4
INH130		0.2	0.8
INH146		> 5	> 10
INH156		2.4	9.4
INH160		5	3.3
INH182		3.5	2
INH56		1.8	4.5

ID	Structure	IC ₅₀ (μM)	
		HeLa	MB468
INH78		0.63	1.4
INH80		2	4.4
INH82		2	2.3
INH136		1.5	3.4
INH154		0.2	0.12
INH168		0.2	0.5
INH174		0.6	0.5
INH212		2.5	2.4

Cells were plated on 96-well dishes one day and then exposed to different concentration of INHs for 4 days. IC₅₀ for INHs was determined by XTT assay as described in Supplementary Materials and Methods.